Conformational changes in the Arp2/3 complex leading to actin nucleation

Avital A Rodal[1,5], Olga Sokolova[2,5], Deborah B Robins[1], Karen M Daugherty[1], Simon Hippenmeyer[3], Howard Riezman[4], Nikolaus Grigorieff[2] & Bruce L Goode[1]

The two actin-related subunits of the Arp2/3 complex, Arp2 and Arp3, are proposed to form a pseudo actin dimer that nucleates actin polymerization. However, in the crystal structure of the inactive complex, they are too far apart to form such a nucleus. Here, we show using EM that yeast and bovine Arp2/3 complexes exist in a distribution among open, intermediate and closed conformations. The crystal structure docks well into the open conformation. The activator WASp binds at the cleft between Arp2 and Arp3, and all WASp-bound complexes are closed. The inhibitor coronin binds near the p35 subunit, and all coronin-bound complexes are open. Activating and loss-of-function mutations in the p35 subunit skew conformational distribution in opposite directions, closed and open, respectively. We conclude that WASp stabilizes p35-dependent closure of the complex, holding Arp2 and Arp3 closer together to nucleate an actin filament.

The rapid assembly of actin filament networks is required for cell locomotion, endocytosis, and the intracellular motility of vesicles, organelles and specific pathogens. At the heart of these processes is the evolutionarily conserved seven-subunit Arp2/3 complex, which directly nucleates actin assembly[1]. The complex is thought to seed actin polymerization by forming a pseudo actin dimer composed of its two actin-related protein subunits, Arp2 and Arp3. However, by itself, the Arp2/3 complex is relatively inactive, and efficient actin nucleation requires its interactions with the WA/VCA domain of a nucleation-promoting factor (NPF), such as SCAR/WASp family proteins and/or a pre-existing (mother) actin filament. These signals stimulate the Arp2/3 complex to nucleate the polymerization of a new (daughter) filament[1]. This tight regulation of the activity of the Arp2/3 complex is thought to be critical *in vivo* for controlling the spatial and temporal assembly of cellular actin filament networks.

The precise mechanism by which the Arp2/3 complex is activated remains poorly understood. The crystal structure of the Arp2/3 complex shows the inactive form, in which there is a large separation between the Arp2 and Arp3 subunits that prohibits formation of a pseudo actin dimer[2]. This observation has led to the proposal that NPFs may induce major structural rearrangements in the Arp2/3 complex to bring the Arp2 and Arp3 subunits closer together[2]. However, experimental evidence for such conformational changes has been limited. Chemical crosslinking of free and NPF-bound Arp2/3 complex reveals differences consistent with conformational changes[3,4]. In addition, a comparison of the structures of free Arp2/3 complex and Arp2/3 complex at filament branchpoints, as determined by cryo-EM and three-dimensional

reconstruction[5], suggests a conformational change coupled to branching. The change occurs in a region of the complex located at the base of the daughter filament. Based on the assumption that Arp2 and Arp3 subunits are located at this end, it was suggested that these changes involve rearrangement of at least one of the actin-related protein subunits (Arp2 or Arp3, or both). However, it was not possible to make a more detailed interpretation because of the resolution of these reconstructions, which precluded specific subunit assignments. As a result, it has not been possible to define the subunit rearrangements that occur upon activation of Arp2/3 complex or to visualize possible transition states.

One limitation of crystallography is that it usually provides the structure of only a single conformation of a protein, when most proteins in solution exist in dynamic equilibrium among several conformations. Here, we used EM and single-particle averaging to image purified yeast and bovine Arp2/3 complexes, because this technique has the potential to detect distinct classes of structures for a protein. We show that the Arp2/3 complex exists in several conformations. The inactive Arp2/3 complex is stabilized in an open conformation, and WASp-mediated closure of the gap between Arp2 and Arp3 primes the complex for actin nucleation.

RESULTS
Arp2/3 complex exists in several conformations
Using EM and single-particle averaging techniques, we imaged purified wild-type *Saccharomyces cerevisiae* Arp2/3 complex (**Fig. 1**). Unlike a previous cryo-EM study on Arp2/3 complex[5], we used negative stain to enhance image contrast and ensure correct alignment and classifica-
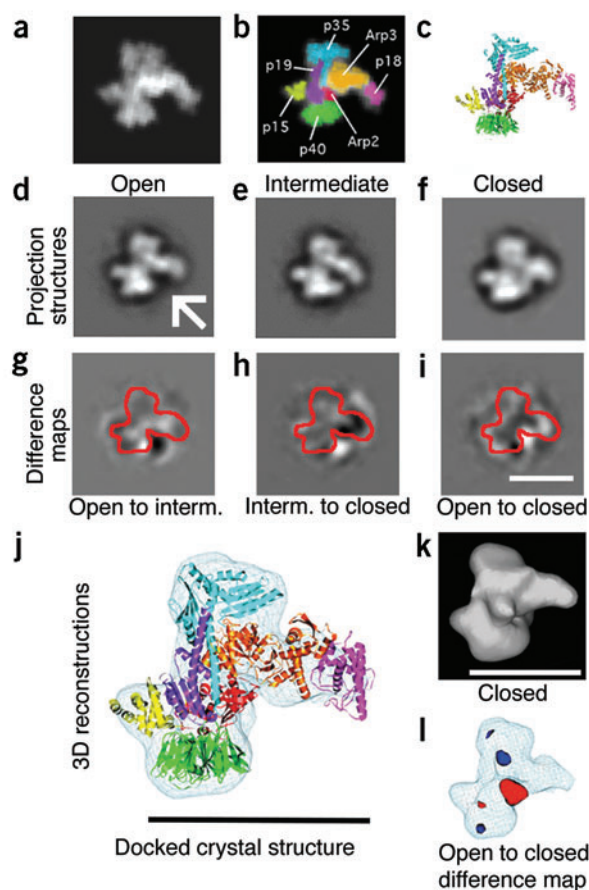
Figure 1 Three different conformations of wild-type Arp2/3 complex. (**a**) Projection map of crystal structure of Arp2/3 complex[2] filtered at a resolution of 20 Å. (**b**) Projection map as in **a**, but with color added to highlight subunits in the complex. (**c**) Crystal structure of the bovine Arp2/3 complex in the same views as in **a** and **b**. (**d**) Projection structure (computed from 1,271 images) of the open conformation. Arrow, major cleft. (**e**) Projection structure (computed from 771 images) of the intermediate conformation. (**f**) Projection structure (computed from 1,150 images) of the closed conformation. (**g**) Difference map of the structures in **d** and **e**. For reference, a red outline of the open projection structure in **d** is shown. (**h**) Difference map of the structures in **e** and **f**. (**i**) Difference map of the structures in **d** and **f**. (**j**) Docking of the Arp2/3 crystal structure into the three-dimensional structure of yeast Arp2/3 complex in the open conformation. (**k**) Three-dimensional structure of the closed conformation. (**l**) Difference map between the three-dimensional structures of the open and closed conformations. Positive densities, red; negative densities, blue. Scale bars, 100 Å.

tion of particles. Classification of *S. cerevisiae* Arp2/3 complex particles revealed three distinct conformations, for which projection maps were generated (**Fig. 1d–f**). The number of distinct classes that contained the vast majority of particles did not depend on the number of classes generated, suggesting that only three conformations existed. This does not rule out the possibility that additional conformations exist but suggests that the three identified are the predominant stable species. The resolution of the projection structures was ~25 Å, estimated by the Fourier ring correlation method (data not shown). We refer to these conformations as 'open,' 'intermediate' and 'closed,' on the basis of differences in the size of the major cleft (arrow in **Fig. 1d**). The three structures were distributed in approximately equal ratios (see below).

For comparison, we created a projection map from the crystal structure of inactive bovine Arp2/3 complex[2] (**Fig. 1a–c**) and found that it closely resembles our open and intermediate conformations (**Fig. 1d,e**). This resemblance is not due to bias introduced into the alignment, because the crystal structure was never used as a reference in processing the data. We could not compare the structures determined here to those previously obtained by cryo-EM[5], because there are no recognizable features in the cryo-EM structures that align with the crystal structure or our negatively stained structures.

The resolution of our experimental projections was notable given the relatively small size of the Arp2/3 complex (231 kDa) and allowed us to assign the positions of each subunit when compared with the crystal structure. The region of the complex that undergoes the most noticeable changes among open, intermediate and closed conformations is located near the Arp2, Arp3 and p18 subunits. The dynamic nature of this region may help to explain why half of Arp2 was disordered and absent from the crystal structure, and a mass that appears in this location

in our intermediate and closed conformations may represent that part of Arp2. The difference map created by subtracting the open from the intermediate conformations suggests that Arp2 moves from the bottom center of the projection in **Figure 1d** toward the bottom right, whereas Arp3 drops toward Arp2, resulting in a loss of mass from the center right (**Fig. 1g**). The difference map created by subtracting the intermediate from the closed conformation revealed a further 'tuck' of Arp2, Arp3 and p18 (bovine p21) from the periphery toward the center of the complex (**Fig. 1h**). The difference map created by subtracting the open from the closed conformation reveals net shifts in the positions of Arp2, Arp3 and p18, resulting in compaction of the complex (**Fig. 1i**). We observed little or no change in the positions of the other four subunits.

To verify that the conformational differences characterizing the open, intermediate and closed states are not merely the result of different views of the complex in the electron microscope, we derived three-dimensional maps for each conformation, aligned them to each other and calculated difference maps. The Arp2/3 crystal structure docks well into the three-dimensional map of the open but not the closed state (**Fig. 1j,k**), consistent with the two-dimensional results. The three-dimensional difference map between the open and closed state (**Fig. 1l**) confirmed that the primary change occurs in the positions of Arp2, Arp3 and p18.

The structure of WASp-bound Arp2/3 complex

To address how NPFs influence Arp2/3 complex conformation, we imaged Arp2/3 complex in the presence of full-length yeast WASp (Las17), which has a stronger Arp2/3-complex binding affinity (data not shown) and nucleation-promoting activity[6] than its WA/VCA domain alone. Four classes of particles were detected, as opposed to three classes in the absence of WASp. All of the particles in the new class (35% of total particles) were in a conformation most similar to the closed conformation and had an additional mass near the protrusion formed by Arp3 and p18 (**Fig. 2**). We interpret this new class as WASp-bound Arp2/3 complex. The remaining 65% of particles aligned well with the previously calculated open, intermediate and closed conformations and probably represent free complex. The difference map generated by subtracting the free closed structure from the new structure shows that the additional mass (arrows, **Fig. 2b,c**) resides at a position on or between Arp2 and Arp3. One possibility is that this mass results solely from marked rearrangements of the Arp2 and Arp3 subunits themselves, but because we never observed such a mass in the three structures of free Arp2/3 complex, we favor the interpretation that the additional mass comes from WASp itself. Furthermore, the location of this mass is consistent with the chemical crosslinking of WASp to p40, Arp2 and Arp3 (refs. 3,4). The new mass is slightly smaller than might be predicted for yeast WASp (67 kDa) and
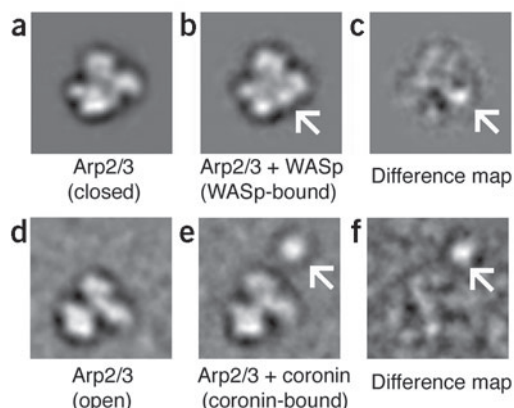
Figure 2 Activated (WASp-bound) Arp2/3 complex is in the closed conformation and inactive (coronin-bound) Arp2/3 complex is in the open conformation. (**a**) Projection structure of Arp2/3 complex in its closed conformation, the same as in **Figure 1f**. (**b**) WASp-bound Arp2/3 complex (computed from 428 images). (**c**) Difference map between the closed conformation and WASp-bound complex. In the WASp-bound structure and the difference map, arrows mark the additional, clearly defined density. (**d**) Projection structure of Arp2/3 complex in its open conformation, the same as in **Figure 1d**. (**e**) Coronin-bound Arp2/3 complex (computed from 877 images). (**f**) Difference map between the open conformation and coronin-bound complex. In the coronin-bound structure and the difference map, arrows mark the additional, clearly defined density.

thus may represent only one well-ordered domain of the protein, whereas other less well-ordered domains might not result in a clear mass after particle averaging. The WASp-bound structure more strongly resembles the free closed conformation than the free open or intermediate conformations, as seen by comparing the difference maps (**Supplementary Fig. 1** online). These data are consistent with a model in which WASp binds near Arp2 and Arp3 and stabilizes the closed conformation.

The structure of coronin-bound Arp2/3 complex

We next imaged Arp2/3 complex in the presence of its direct inhibitor, coronin[7]. A total of 69% of particles aligned well with the open, intermediate and closed conformations, again probably representing free complex. The remaining particles fell into classes that were most similar to the open conformation but showed additional density near the p35 subunit. Because these classes were visible only in the presence of coronin, they probably represent coronin-bound Arp2/3 complex (**Fig. 2e**). The detection of these new open structures is the opposite result from imaging WASp and Arp2/3 complex, which produced a new closed structure. The difference map (**Fig. 2f**) generated by subtracting the free open structure (**Fig. 2d**) from the most prominent of the new open coronin-bound structures showed a new mass ~40 Å in diameter (arrows, **Fig. 2e,f**) that resides ~20 Å from the p35 subunit. This mass probably represents the largest domain of coronin, its 40-kDa WD-repeat region, which is predicted to form a β-propeller structure. This domain does not participate in interactions with Arp2/3 complex[7], so it is not surprising that it does not directly contact the complex. Instead, a short (50-residue) coiled-coil domain located at the C terminus of coronin has been shown to mediate both the physical association with and inhibition of Arp2/3 complex[7]. In the primary structure of yeast coronin, the coiled-coil domain is separated from the β-propeller by a 20-kDa central region of unknown structure. This segment may account for the 20-Å spacing of the coronin β-propeller from p35. The proximity of the visible coronin mass to the p35 subunit is consistent with reported physical interactions between the coiled-coil domain and p35 (ref. 7). Together, the data indicate that coronin binds near p35 and stabilizes the open conformation of Arp2/3 complex to inhibit nucleation activity.
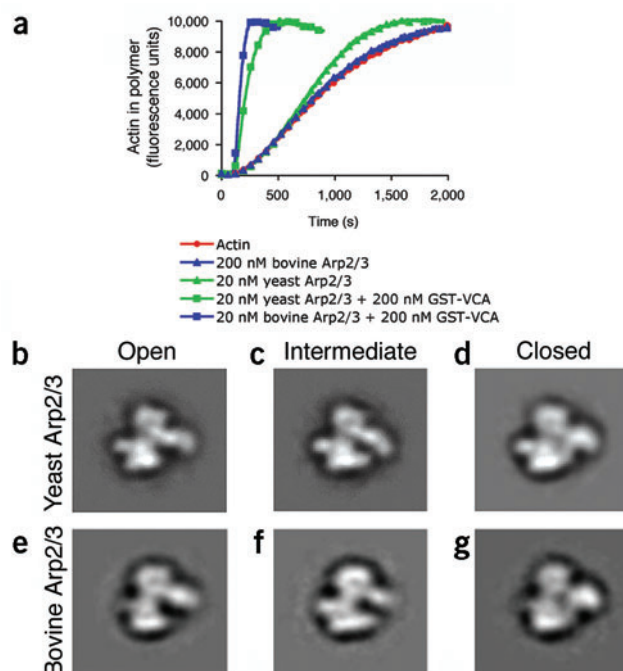
Comparison of yeast and bovine Arp2/3 complex

To address whether Arp2/3 complexes from other species have similar conformations to yeast Arp2/3 complex, we imaged bovine Arp2/3 complex. First, we directly compared the actin nucleation activities of bovine and *S. cerevisiae* Arp2/3 complexes. The two were activated equally using a WA/VCA fragment of mammalian WASp; however, the *S. cerevisiae* complex had a more 'leaky' or constitutive activity in the absence of activator compared with bovine Arp2/3 complex (**Fig. 3a**). We then generated single-particle averages of bovine Arp2/3 complex and compared them with the averages of yeast Arp2/3 complex (**Fig. 3b–g**). Although its subunits share only ~50% amino acid sequence identity with their yeast counterparts, the single-particle averages of bovine Arp2/3 complex were similar to yeast Arp2/3 complex and classified similarly into three conformations: open, intermediate and closed. Consistent with its lower spontaneous nucleation activity, the bovine Arp2/3 complex had a skewed conformational distribution toward the open state compared with yeast complex, with 60% of particles open and only 18% closed. These correlative data further support the assignment of the open conformation as inactive.

Role of p35 subunit in activation of Arp2/3 complex

Activation of the Arp2/3 complex is thought to involve interactions both with NPFs and the sides of mother filaments[1,8–10], and these signals may be coordinated to act additively, in a specific temporal order,

Figure 3 Bovine Arp2/3 complex is suppressed for spontaneous activity and is skewed toward the open conformation. (**a**) Bovine Arp2/3 complex is suppressed for spontaneous nucleation activity. Rabbit skeletal muscle actin (3 μM, 1% pyrene-labeled) was polymerized in the presence of the indicated concentrations of yeast or bovine Arp2/3 complex and GST-WA/VCA fragment of human N-WASp. (**b–g**) Comparison of projection structures of yeast Arp2/3 complex (**b–d**) with those of bovine Arp2/3 complex (**e–g**) (computed from 2,042 images).
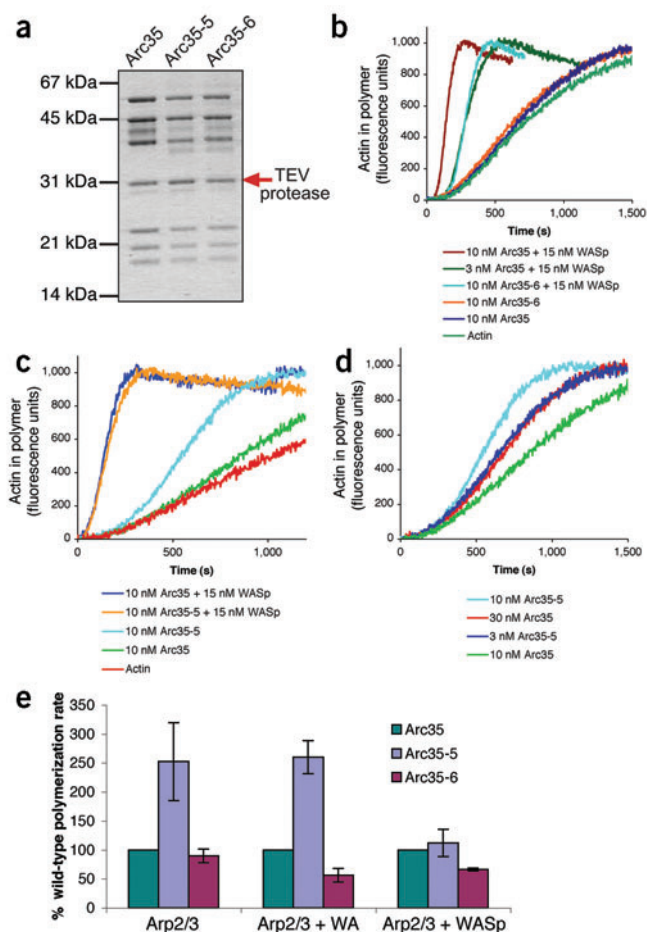
Figure 4 Actin nucleation activities of mutant and wild-type Arp2/3 complexes. (**a**) Coomassie-stained gel of purified wild-type and mutant Arp2/3 complexes. (**b**–**d**) Rabbit skeletal muscle actin (3 µM, 1% pyrene-labeled) was polymerized in the presence of 10 nM Arp2/3 complex and 15 nM yeast WASp or 400 nM WA fragment of yeast WASp. (**e**) The rate of polymerization was calculated from the slope of assembly curves in **b**–**d** at 50% polymerization, where the curves are linear, and rates of assembly for mutant Arp2/3 complexes were normalized to the assembly rate for similarly activated wild-type Arp2/3 complex.

in vitro, consistent with reduced affinity for WASp (J. D'Agostino, Brandeis University, and B.G., unpublished results).

In contrast to Arc35-6, Arc35-5 had pronounced leaky or constitutive actin nucleation activity in the absence of any NPF. Furthermore, Arc35-5 was more strongly activated than wild-type Arp2/3 complex by WA fragment, but not by WASp (**Fig. 4c–e**). Arc35-5, in the absence of any NPF, had activity comparable to a ten-fold higher concentration of wild-type Arp2/3 complex (**Fig. 4d**). Our preparations contained no contaminating WASp (**Supplementary Fig. 4** online). These observations demonstrate that mutations in Arc35-5 partially mimic activated Arp2/3 complex, whereas mutations in Arc35-6 partially impair responsiveness to WASp, but not because of defects in NPF binding.

We compared the structures of Arp2/3 complex isolated in two independent preparations each from wild-type, *arc35-5* and *arc35-6* strains. The abundance of intermediate conformation was constant within the error margins for wild type and both mutants. However, the abundance of open and closed conformations differed substantially among Arc35-6 (loss of function), Arc35 (wild type) and Arc35-5 (constitutively active) (**Fig. 5a**). The prevalence of the open conformation in Arc35-6 supports further our assignment of this conformation as inactive. The prevalence of the closed conformation in Arc35-5 supports further our assignment of this conformation as primed for activation. It is not surprising that the *arc35* mutants we isolated from our temperature-sensitive screen are only partially skewed toward the open or closed conformations, because mutations causing a more severe bias would probably be lethal *in vivo*.

DISCUSSION

We draw three major conclusions from our data. First, the Arp2/3 complex is in equilibrium among several conformations ranging from open to closed. Second, the p35 subunit has an important role in regulating transitions between the open and closed conformations. Third, the open conformation represents an inactive state, and transition to the closed conformation primes the complex for actin nucleation. These activity assignments for the open and closed conformations are supported by several observations: (i) 100% of Arp2/3-complex molecules bound by the activator WASp are closed; (ii) 100% of Arp2/3-complex molecules bound by the inhibitor coronin are open; (iii) the inactive crystal structure of bovine Arp2/3 complex docks well into our two-dimensional and three-dimensional reconstructions of the open but not the closed conformation; (iv) in the absence of WASp, bovine Arp2/3 complex has reduced spontaneous actin nucleation activity compared with yeast Arp2/3 complex, and a corresponding skewed distribution toward the open conformation; (v) inactivating mutants in the p35 subunit of the Arp2/3 complex show a shifted distribution of particles toward the open conformation, whereas activating mutants show a shifted distribution toward the closed conformation.

In our model, the p35 subunit has a pivotal role in relaying activation signals to other subunits in the complex. This is demonstrated in two ways: first, different mutations in this subunit can have opposite effects on activity and conformation. Second, coronin binds near p35 and shifts 100% of Arp2/3-complex molecules to which it is bound into the open conformation (**Fig. 5a**). At present, it remains unclear

or both, to influence Arp2/3 complex structure. The p35 subunit is not predicted to participate directly in actin nucleation or to bind NPFs. However, p35 is required for structural integrity of the complex and serves as a hub, making direct contacts with the sides of mother filaments, three other subunits in the complex (p19, Arp2 and Arp3) and the inhibitor coronin[2,7,8,10,11]. Thus, p35 is in a prime position to receive several regulatory inputs and relay conformational changes to Arp2 and Arp3 subunits to signal activation or inhibition of nucleation. Using a random mutagenesis strategy, we isolated temperature-sensitive alleles of *ARC35*, the essential gene in *S. cerevisiae* that encodes p35. Sequencing showed that each allele contained five to eight substitutions of single amino acid residues (**Supplementary Fig. 2** online). We purified Arp2/3 complex from the wild-type strain and >12 *arc35* mutant strains (examples in **Fig. 4a**) and compared their actin nucleation activities alone and in the presence of full-length yeast WASp (**Fig. 4b–e**) or its WA/VCA domain (**Fig. 4e**).

The actin nucleation activities of the mutants fell into two separate classes, typified by Arc35-5 and Arc35-6. Arc35-6 is impaired for activation by both full-length WASp and WA fragment (**Fig. 4b,e**). When stimulated by WASp, Arc35-6 had the same activity as a three-fold lower concentration of wild-type Arp2/3 complex (**Fig. 4b**). Arc35-6 responded similarly to wild-type Arp2/3 complex to increasing WASp concentrations (**Supplementary Fig. 3** online), suggesting that it does not simply have reduced affinity for WASp. In contrast, a nucleation-impaired mutation in the Arp2 subunit, which is predicted to bind to WASp, is rescued by elevating WASp concentrations *in vivo* and
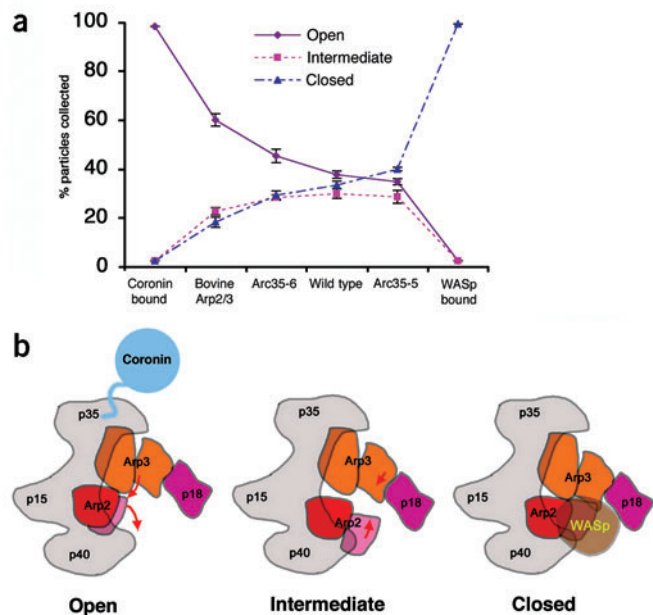
Figure 5 Conformational states of the Arp2/3 complex. (**a**) Correlation between activity and distribution of Arp2/3 complex among the three conformations. Error bars show s.d. derived from four data sets for each point, except for bovine Arp2/3 complex, for which seven data sets were used. (**b**) Model for structural rearrangements during activation of the Arp2/3 complex. Arrows indicate conformational changes leading to the next structure in the activation sequence. In the transition from the open to the intermediate conformation, Arp2 and Arp3 subunits move toward the center of the gap separating the two subunits. Next, there is a further closure of the gap between Arp2 and Arp3 by a movement of Arp2 toward Arp3, and possibly a small movement of Arc18 toward the center of the gap, creating the closed conformation. WASp is shown binding to Arp2 and Arp3, and possibly also to p40, stabilizing the closed conformation. Coronin is shown binding to p35, stabilizing the open conformation.

how p35 helps induce structural rearrangements in Arp2, Arp3 and p18. However, one possibility is that signals are relayed through the long C-terminal helix of p35, which extends toward Arp2 in the crystal structure[2]. In fact, the contacts between p35 and Arp2 may be even more extensive, because a considerable stretch of the p35 C terminus is missing from the crystal structure (16 amino acids of bovine p35 and a corresponding 27 residues of *S. cerevisiae* p35). The p35 sub-unit also is implicated in binding to the sides of filaments[8,10,11], and filament-side binding contributes to WA/VCA-induced activation[9,10,12]. Thus, the mutations in Arc35-5 and Arc35-6 may partially mimic the filament-bound and filament-free conformations of Arp2/3 complex, respectively. This proposal is consistent with our actin assembly kinetics results. Arc35-5 remains more active than wild-type Arp2/3 complex when stimulated by the WA/VCA domain but not WASp (**Fig. 4e**), suggesting that WA/VCA-independent aspects of WASp activation are constitutive in this mutant. A putative actin filament–binding domain in the N terminus of WASp[13,14] may recruit Arp2/3 complex to filament sides, masking the effects of Arc35-5.

Our data suggest an actin nucleation mechanism in which WASP and filament-bound p35 stabilize the closed conformation of Arp2/3 complex, holding Arp2 and Arp3 close together to promote actin nucleation (**Fig. 5b**). Our model for closure of the Arp2/3 complex is consistent with reported differences in the chemical crosslinking patterns of free and NPF-bound Arp2/3 complex[3,4], with differences in the cryo-EM structures of free Arp2/3 complex and Arp2/3 complex at filament

branchpoints[5], and with NMR and photo crosslinking data showing that the central acidic (CA) region of WASp binds to Arp2, Arp3 and p18 (M. Rosen, University of Texas Southwestern Medical Center at Dallas, personal communication). Our results also agree with the general predictions of Robinson and colleagues[2] but show that the subunit movements are more complex than the suggested simple rigid-body rotation. It should be emphasized that although closure of the complex represents a key step in the activation mechanism, it is not sufficient to promote strong actin nucleation. In addition to stabilizing the closed conformation of the Arp2/3 complex, WASp must provide an actin monomer to the barbed ends of the Arp subunits[1], and WASP and/or actin binding are required to alter the nucleotide-bound state of Arp subunits to promote actin nucleation[15–18]. Future structural analyses of the Arp2/3 complex in different nucleotide-bound states, and bound to both WASp and an actin monomer, should help clarify the precise mechanism for actin nucleation.

METHODS

Generation of arc35 mutant strains. A centromere-based plasmid (YEPlac211; ref. 19) containing genomic DNA 125 base pairs (bp) upstream to 500 bp downstream of the *ARC35* open reading frame (ORF) was mutagenized by error-prone PCR and transformed into an *arc35Δ* strain carrying *pLYS2-ARC35*. Transformants were plated on α-aminoadipic acid to select against *pLYS2-ARC35*. Mutant plasmids were rescued, and mutagenized *ARC35* genomic fragments were subcloned into XbaI and PstI sites of pRS305 and integrated at the *LEU2* locus of strain BGY848 (*MATa, leu2, ura3, his3, ARP2:TEV3xHA:HISMX, arc35Δ: KANMX, pRS316-ARC35*). *URA3*-marked *pRS316-ARC35* was removed by plating transformants on 5-fluoroorotic acid. The *ARC35* ORF was amplified from these strains by PCR and sequenced.

Protein purification. Arp2/3 complex was purified from strains expressing mutant Arc35 alleles as their only source of Arc35 (described earlier) and Arp2 tagged with a TEV protease site followed by three copies of the hemagglutinin (HA) epitope as their only source of Arp2. Frozen yeast were lysed as described[6] and thawed in a 1:1 (w/v) ratio of HEK buffer (20 mM HEPES, pH 7.5, 1 mM EDTA, 50 mM KCl) with protease inhibitors[6] and 0.5% (v/v) Triton X-100. Lysate (18 ml) was cleared for 20 min at 80,000 r.p.m. (260,000*g*) in a TLA100.3 rotor (Beckman) and incubated for 1.5 h with HA antibody-coated beads[6]. Beads were washed with 15 ml HEK + 0.5% (v/v) Triton X-100, 15 ml HEK + 450 mM KCl and 15 ml HEK, then resuspended in 200 µl HEK and 3 units of rTEV protease (Invitrogen). After 1 h of incubation at room temperature, 3 additional units of rTEV were added and proteins were incubated again for 1 h. The supernatant was removed and flash-frozen in liquid N$_2$. rTEV has no effect on actin polymerization mediated by Arp2/3 complex[6]. Bovine Arp2/3 complex and GST-VCA[20], yeast coronin[7], full-length yeast WASp (Las17)[6] and its WA fragment[21] were purified as described. Rabbit skeletal muscle actin (unlabeled and pyrene-labeled) was purchased from Cytoskeleton.

Actin assembly kinetics. Actin assembly reactions contained 3 µM rabbit skeletal muscle actin (1% pyrene-labeled) and were carried out in a PTI spectrofluorometer. Monomeric actin (22.5 µM) was mixed with the relevant proteins at the indicated concentrations and added to initiation salts (final concentration F buffer: 10 mM Tris, pH 7.5, 0.2 mM DTT, 0.2 mM CaCl$_2$, 100 mM KCl, 0.5 mM ATP, 2 mM MgCl$_2$). The rate of polymerization was calculated from the slope of assembly curves at 50% polymerization.

EM and single-particle analysis. Preparations of Arp2/3 complex were diluted to 0.25 µM with HEK and applied to glow-discharged carbon-coated copper 400-mesh grids. Excess protein solution was blotted away, and specimens were negatively contrasted with 0.75% (w/v) uranyl formate in water (yeast Arp2/3, free and bound to WASp) or with 1% (w/v) uranyl acetate in water (yeast Arp2/3 bound to coronin and bovine Arp2/3). Grids were examined in a Philips CM12 electron microscope at 120 kV under low-dose conditions. Negatives were taken at 45,000× magnification and an image defocus of 1.8 µm, and scanned on a Zeiss SCAI scanner, using a pixel size of 7 µm. After 3 × 3 pixel averaging, the pixel size on the specimen was 4.67 Å pixel^{-1}. A typical field is shown in **Supplementary Figure 5** online.

Particles were manually selected from 15 negatives of wild-type Arp2/3 complex and two mutants (Arc35-5 and Arc35-6). A total of 3,192 particles were processed using the IMAGIC package[22]. Classification into six classes yielded three distinct classes that contained the majority of particles representing three conformations of the protein. The three remaining classes each contained ≤5% of the particles from the data set, showed no similarity to the Arp2/3 complex crystal structure[2] and were discarded. The three primary classes were used as the new references for multiple-reference alignment of the data set, yielding improved classes. A second set of 3,735 particles was processed independently under identical conditions, giving classes that were virtually indistinguishable from the first data set. The second data set was used to estimate the errors in the distributions determined for the three conformations of the complex. Difference maps were calculated after scaling each projection structure to give the same variance and zero mean. The Fourier ring correlation[23], calculated between projection structures that each included one-half of the data, was used to estimate the resolution of the projection structures. The resolution of all structures was estimated at 25 Å, corresponding approximately to the first zero of the contrast transfer function of the electron microscope.

To image Arp2/3 complex bound to WASp or coronin, the complex and WASp or coronin were mixed at a 1:1 molar ratio and applied to copper 400-mesh grids as before. For WASp, manual selection from 18 negatives yielded 1,408 images in one data set and 1,756 images in a second data set. Particles were classified as before, yielding only four strong classes. Three of these classes were virtually indistinguishable from the previously obtained classes. The difference maps between the closed conformation of unbound Arp2/3 complex and the WASp-bound complex, and the open conformation and the coronin-bound complex were calculated as described earlier.

Three-dimensional reconstructions of the open, intermediate and closed states were determined using the random conical tilt method[24,25], as implemented in the SPIDER[25]. Particles were selected from images of specimens tilted at 0° and 45°. The data sets contained 1,025 tilt pairs for closed conformation, 988 tilt pairs for open conformation and 762 tilt pairs for the intermediate conformation. Refinement and correction for the contrast transfer function of the electron microscope were done using FREALIGN[26], resulting in three-dimensional structures with a resolution of 25 Å. The three-dimensional difference maps were calculated using IMAGIC[22] after alignment of the structures to each other by maximization of a correlation coefficient. All three-dimensional maps were visualized using the molecular viewer CHIMERA[27]. The Arp2/3 crystal structure was docked into the three-dimensional map of the open conformation using SITUS[28]; the best match gave a correlation coefficient of 0.3.

1. Welch, M.D. & Mullins, R.D. Cellular control of actin nucleation. *Annu. Rev. Cell Dev. Biol.* **18**, 247–288 (2002).
2. Robinson, R.C. *et al.* Crystal structure of Arp2/3 complex. *Science* **294**, 1679–1684 (2001).
3. Zalevsky, J., Lempert, L., Kranitz, H. & Mullins, R.D. Different WASP family proteins stimulate different Arp2/3 complex-dependent actin-nucleating activities. *Curr. Biol.* **11**, 1903–1913 (2001).
4. Weaver, A.M. *et al.* Interaction of cortactin and N-WASp with Arp2/3 complex. *Curr. Biol.* **12**, 1270–1278 (2002).
5. Volkmann, N. *et al.* Structure of Arp2/3 complex in its activated state and in actin filament branch junctions. *Science* **293**, 2456–2459 (2001).
6. Rodal, A.A., Manning, A.L., Goode, B.L. & Drubin, D.G. Negative regulation of yeast WASp by two SH3 domain-containing proteins. *Curr. Biol.* **13**, 1000–1008 (2003).
7. Humphries, C.L. *et al.* Direct regulation of Arp2/3 complex activity and function by the actin binding protein coronin. *J. Cell Biol.* **159**, 993–1004 (2002).
8. Mullins, R.D., Stafford, W.F. & Pollard, T.D. Structure, subunit topology, and actin-binding activity of the Arp2/3 complex from *Acanthamoeba*. *J. Cell Biol.* **136**, 331–343 (1997).
9. Machesky, L.M. *et al.* Scar, a WASp-related protein, activates nucleation of actin filaments by the Arp2/3 complex. *Proc. Natl. Acad. Sci. USA* **96**, 3739–3744 (1999).
10. Bailly, M. *et al.* The F-actin side binding activity of the Arp2/3 complex is essential for actin nucleation and lamellipod extension. *Curr. Biol.* **11**, 620–625 (2001).
11. Gournier, H., Goley, E.D., Niederstrasser, H., Trinh, T. & Welch, M.D. Reconstitution of human Arp2/3 complex reveals critical roles of individual subunits in complex structure and activity. *Mol. Cell* **8**, 1041–1052 (2001).
12. Pantaloni, D., Boujemaa, R., Didry, D., Gounon, P. & Carlier, M.F. The Arp2/3 complex branches filament barbed ends: functional antagonism with capping protein. *Nat. Cell Biol.* **2**, 385–391 (2000).
13. Suetsugu, S., Miki, H., Yamaguchi, H., Obinata, T., & Takenawa, T. Enhancement of branching efficiency by the actin filament-binding activity of N-WASP/WAVE2. *J. Cell Sci.* **114**, 4533–4542 (2001).
14. Egile, C. *et al.* Activation of the CDC42 effector N-WASP by the *Shigella flexneri* IcsA protein promotes actin nucleation by Arp2/3 complex and bacterial actin-based motility. *J. Cell Biol.* **146**, 1319–1332 (1999).
15. Dayel, M.J., Holleran, E.A. & Mullins, R.D. Arp2/3 complex requires hydrolyzable ATP for nucleation of new actin filaments. *Proc. Natl. Acad. Sci. USA* **98**, 14871–14876 (2001).
16. Le Clainche, C., Didry, D., Carlier, M.F. & Pantaloni, D. Activation of Arp2/3 complex by Wiskott-Aldrich syndrome protein is linked to enhanced binding of ATP to Arp2. *J. Biol. Chem.* **276**, 46689–46692 (2001).
17. Le Clainche, C., Pantaloni, D. & Carlier, M.F. ATP hydrolysis on actin-related protein 2/3 complex causes debranching of dendritic actin arrays. *Proc. Natl. Acad. Sci. USA* **100**, 6337–6342 (2003).
18. Dayel, M.J. & Mullins, R.D. Activation of Arp2/3 complex: addition of the first subunit of the new filament by a WASP protein triggers rapid ATP hydrolysis on Arp2. *PLoS Biol.* **2**, E91 (2004).
19. Gietz, R.D. & Sugino, A. New yeast–*Escherichia coli* shuttle vectors constructed with *in vitro* mutagenized yeast genes lacking six–base pair restriction sites. *Gene* **74**, 527–534 (1988).
20. Higgs, H.N. & Pollard, T.D. Activation by Cdc42 and PIP(2) of Wiskott-Aldrich syndrome protein (WASp) stimulates actin nucleation by Arp2/3 complex. *J. Cell Biol.* **150**, 1311–1320 (2000).
21. Winter, D., Lechler, T. & Li, R. Activation of the yeast Arp2/3 complex by Bee1p, a WASP-family protein. *Curr. Biol.* **9**, 501–504 (1999).
22. Van Heel, M., Harauz, G., Orlova, E.V., Schmidt, R. & Schatz, M. A new generation of the IMAGIC image processing system. *J. Struct. Biol.* **116**, 17–24 (1996).
23. Harauz, G. & van Heel, M. Exact filters for general geometry three-dimensional reconstruction. *Optik* **73**, 146–156 (1986).
24. Frank, J. & Radermacher, M. Three-dimensional reconstruction of single particles negatively stained or in vitreous ice. *Ultramicroscopy* **46**, 241–262 (1992).
25. Frank, J. *et al.* SPIDER and WEB: processing and visualization of images in 3D electron microscopy and related fields. *J. Struct. Biol.* **116**, 190–199 (1996).
26. Grigorieff, N. Three-dimensional structure of bovine NADH:ubiquinone oxidoreductase (complex I) at 22 Å in ice. *J. Mol. Biol.* **277**, 1033–1046 (1998).
27. Huang, C.C., Couch, G.S., Pettersen, E.F. & Ferrin, T.E. Chimera: an extensible molecular modeling application constructed using standard components. *Pac. Symp. Biocomput.* **1**, 724 (1996).
28. Wriggers, W., Milligan, R. & McCammon, J. Situs: a package for docking crystal structures into low-resolution maps from electron microscopy. *J. Struct. Biol.* **125**, 185–195 (1999).